Multi-frequency direct sampling method in inverse scattering problem
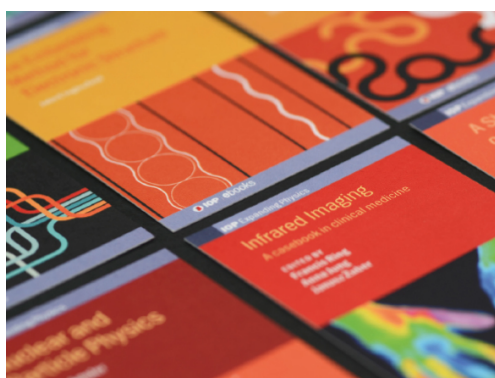
Sangwoo Kang, Marc Lambert, Won-Kwang Park

Multi-frequency direct sampling method in inverse scattering problem

To cite this article: Sangwoo Kang *et al* 2017 *J. Phys.: Conf. Ser.* **904** 012018

View the article online for updates and enhancements.

Multi-frequency direct sampling method in inverse scattering problem

Sangwoo Kang[1], Marc Lambert[1], and Won-Kwang Park[2]

[1]Group of Electrical Engineering, Paris (GeePs),UMR CNRS 8507, CentraleSupélec, Univ. Paris Sud, Université. Paris Saclay, UPMC Univ Paris 06, 3 & 11 rue Joliot-Curie 91192, Gif-sur-Yvette, France.
[2]Department of Information Security, Cryptology, and Mathematics, Kookmin University, Seoul, 02707, Korea

E-mail: `sangwoo.kang@geeps.centralesupelec.fr`, `parkwk@kookmin.ac.kr` and `marc.lambert@geeps.centralesupelec.fr`

Abstract. We consider the direct sampling method (DSM) for the two-dimensional inverse scattering problem. Although DSM is fast, stable, and effective, some phenomena remain unexplained by the existing results. We show that the imaging function of the direct sampling method can be expressed by a Bessel function of order zero. We also clarify the previously unexplained imaging phenomena and suggest multi-frequency DSM to overcome traditional DSM. Our method is evaluated in simulation studies using both single and multiple frequencies.

1. Introduction

This study considers the imaging of two-dimensional electromagnetic inclusions within a homogeneous space. The imaging is performed on measured scattered field data. Various non-iterative imaging algorithms have already been developed for this purpose, such as MUltiple SIgnal Classification [1, 2], the linear sampling method [3, 4], and Kirchhoff and subspace migrations [5, 6]. Although these methods are very effective for imaging unknown targets, they usually yield poor results when the number of incident waves is limited to one or only a few.

To overcome this difficulty, researchers have investigated the direct sampling method (DSM). According to [7, 8, 9], DSM has some merits: (i) it requires only one or a few incident waves for imaging the shapes and locations of unknown inclusions, (ii) it performs without any matrix operation (such as singular value decomposition), and (iii) it is highly tolerant to noise. However, these advantages are tempered by several drawbacks: (i) the direction of propagation is crucial for identifying the shapes and locations of inclusions, (ii) there are many artifacts in the map of DSM, and (iii) an inclusion with significantly smaller size or permittivity than other inclusions is difficult to identify by DSM.

To overcome these limitations, we improve the traditional DSM by applying multiple frequencies. The effectiveness of the technique is demonstrated on various synthetic and experimental data. The results confirm that the suggested imaging technique identifies unknown targets with dielectric contrast against the background space and improves the traditional DSM.

The remainder of the study is structured as follows. Section 2 introduces the two-dimensional direct scattering problem in the presence of small dielectric inhomogeneities. In section 3, we

briefly review single-frequency DSM, show that DSM can be expressed by a Bessel function of order zero, and propose our multi-frequency-based DSM. Section 4 presents the numerical and experimental results of both single and multiple frequency evaluations, and section 5 provides a short conclusion.

2. Two-dimensional direct scattering problem

In this section, we consider two-dimensional direct scattering from small dielectric inclusions τ_m, represented as $\tau_m = \mathbf{y}_m + \alpha_m \mathbf{B}_m$, $m = 1, 2, \cdots, M$. Let τ be the set of these scatterings; i.e., $\tau = \bigcup_m \tau_m$. For simplicity, we assume that all τ_m are balls with radius α_m located at $\mathbf{y}_m$. We also assume that $\mathbf{B}_m$ is a simply connected domain (circle). Let ω be the angular frequency and ε_m and μ_m be the dielectric permittivity and magnetic permeability of τ_m, respectively. ε_0 and μ_0 are defined analogously. In this paper, we consider only the permittivity contrast case, i.e., we set $\mu_m \equiv \mu_0 = 1$. Then we can define the piecewise constant permittivity $\varepsilon(\mathbf{x})$ as follows:

$$\varepsilon(\mathbf{x}) = \begin{cases} \varepsilon_m, & \text{if} \quad \mathbf{x} \in \tau_m \\ \varepsilon_0, & \text{if} \quad \mathbf{x} \in \mathbb{R}^2 \backslash \overline{\tau}. \end{cases} \tag{1}$$

For simplicity, we set $\varepsilon_0 = 1$. The wavenumber k is then given by $k = \omega\sqrt{\varepsilon\mu} = 2\pi/\lambda$, where λ is the wavelength. We assume that $\alpha_m \ll \lambda$ for all m and $k|\mathbf{y}_m - \mathbf{y}_{m'}| \gg 0.25$ for $m \neq m'$. This means that the τ_ms are well-separated from each other.

Let $u(\mathbf{x}; k)$ be the time-harmonic total field satisfying the following Helmholtz equation:

$$\Delta u(\mathbf{x}; k) + \omega^2 \varepsilon(\mathbf{x}) u(\mathbf{x}; k) = 0 \quad \text{in} \quad \mathbb{R}^2 \backslash \overline{\tau}, \tag{2}$$

with transmission conditions on the boundaries $\partial\tau_m$ for all m. As is well-known, the total field $u(\mathbf{x}; k)$ can be decomposed into an incident field $u^i(\mathbf{x}; k)$ and a scattered field $u^s(\mathbf{x}; k)$ such that $u(\mathbf{x}; k) = u^i(\mathbf{x}; k) + u^s(\mathbf{x}; k)$. In this study, we consider plane-wave illumination, i.e., we let $u^i(\mathbf{x}; k) = e^{ik\mathbf{x} \cdot \mathbf{d}}$ be the incident field with propagation direction $\mathbf{d} \in \mathbb{S}^1$. Here, $\mathbb{S}^1$ denotes the two-dimensional unit circle. Note that $u^s(\mathbf{x}; k)$ satisfies the Sommerfeld radiation condition

$$\lim_{\mathbf{r} \to \infty} \left(\frac{\partial u^s(\mathbf{x}; k)}{\partial \mathbf{r}} - iku^s(\mathbf{x}; k) \right) = 0$$

uniformly in all directions $\mathbf{r} = |\mathbf{x}| \longrightarrow +\infty$. We assume that $u^s(\mathbf{x}_j; k)$, $j = 1, 2, \cdots, J$, is measured on a simply connected curve Γ. For simplicity, we set Γ as a circle with a large radius a such that, for $\mathbf{x} \in \Gamma$ and $m = 1, 2, \cdots, M$, $k|\mathbf{y}_m - \mathbf{x}| \gg 0.25$.

Based on small volume expansion(See [10]), $u^s(\mathbf{x}; k)$ can be expressed as the following asymptotic expansion formula for $j = 1, 2, \cdots, J$:

$$u^s(\mathbf{x}_j) = \sum_{m=1}^{M} \alpha_m^2 (\varepsilon_m - \varepsilon_0) |\mathbf{B}_m| e^{ik\mathbf{d} \cdot \mathbf{y}_m} \Phi(\mathbf{x}_j, \mathbf{y}_m) + O(\alpha_m^2), \tag{3}$$

where $\Phi(\mathbf{x}, \mathbf{y})$ is the two-dimensional fundamental solution

$$\Phi(\mathbf{x}, \mathbf{z}) = \frac{i}{4} H_0^1(k|\mathbf{x} - \mathbf{z}|). \tag{4}$$

3. Single- and multi-frequency direct sampling method

In this section, we briefly survey the DSM developed in [7], introduce the representative formula of the DSM imaging function, and propose a multi-frequency DSM to improve the imaging performance. The imaging function of the DSM is defined as

$$\mathcal{I}_{\text{SF}}(\mathbf{z}; k) = \frac{|\langle u^s(\mathbf{x}_j; k), \Phi(\mathbf{x}_j, \mathbf{z}) \rangle_{L^2(\Gamma)}|}{\|u^s(\mathbf{x}_j; k)\|_{L^2(\Gamma)} \|\Phi(\mathbf{x}_j, \mathbf{z})\|_{L^2(\Gamma)}}, \tag{5}$$

where

$$\langle a(\mathbf{x}_j), b(\mathbf{x}_j)\rangle_{L^2(\Gamma)} := \sum_{j=1}^{J} a(\mathbf{x}_j)\overline{b(\mathbf{x}_j)} = \int_{\Gamma} a(\mathbf{x})\overline{b(\mathbf{x})}d\mathbf{x} \quad \text{and} \quad \|a(\mathbf{x}_j)\| := \langle a(\mathbf{x}_j), a(\mathbf{x}_j)\rangle_{L^2(\Gamma)}.$$

Referring to [7], DSM postulates that $u^s(\mathbf{x})$ can be approximated as

$$u^s(\mathbf{x}) \approx \sum_{m=1}^{M} W_m \Phi(\mathbf{x}, \mathbf{y}_m),$$

where W_m denotes the weight corresponding to τ_m. Then the following relation

$$\int_{\Gamma} u^s(\mathbf{z})\overline{\Phi}(\mathbf{z}, \mathbf{x})\mathrm{d}S \approx \frac{1}{k}\sum_{m=1}^{M} W_m \mathrm{Im}\left(\Phi(\mathbf{y}_m, \mathbf{x})\right) \approx \frac{1}{k}\sum_{m=1}^{M} J_0(k|\mathbf{z} - \mathbf{y}_m|), \tag{6}$$

we can observe that

$$\mathcal{I}_{\mathrm{SF}}(\mathbf{z}; k) \propto \sum_{m=1}^{M} J_0(k|\mathbf{z} - \mathbf{y}_m|).$$

From the above, we can see that if $\mathbf{z} = \mathbf{y}_m \in \tau_m$, then $\mathcal{I}(\mathbf{z}) \approx 1$, whereas if $\mathbf{z} \notin \tau$, then $\mathcal{I}(\mathbf{z}) < 1$. Therefore, we can identify the locations of τ_m by finding the $\mathbf{y}$ such that $\mathcal{I}(\mathbf{z}) \approx 1$. This method seems to be entirely reasonable, but leaves some phenomena unexplained. For example, τ_m with relatively small size or permittivity are very difficult to locate by this method. Motivated by this fact, we derive the following representation of $\mathcal{I}_{\mathrm{SF}}(\mathbf{z}; k)$ where the maximum value comes from the Hölder inequality. A detailed derivation will appear in an extended version of this study.

$$\mathcal{I}_{\mathrm{SF}}(\mathbf{z}; k) = \left|\sum_{m=1}^{M} \alpha_m^2(\varepsilon_m - \varepsilon_0)|\mathbf{B}_m|J_0(k|\mathbf{z} - \mathbf{y}_m|)\right|\left(\max\left|\sum_{m=1}^{M} \alpha_m^2(\varepsilon_m - \varepsilon_0)|\mathbf{B}_m|\right|\right)^{-1}. \tag{7}$$

As evident in (7), a τ_m with smaller size or permittivity than the other τ_ms will be difficult to locate because $\mathcal{I}_{\mathrm{SF}}(\mathbf{z}; k)$ is maximized at the inclusion with largest size or permittivity.

To overcome this difficulty, we exploit the well-known fact that multiple frequencies guarantee better results than single-frequency applications [5, 6]. Therefore, we introduce the following multi-frequency DSM. For N-different wavenumbers k_n, $n = 1, \cdots, N$, the imaging function can be introduced as

$$\mathcal{I}_{\mathrm{MF}}(\mathbf{z}) = \frac{1}{N}\left|\sum_{n=1}^{N} \langle u^s(\mathbf{x}_j; k), \Phi(\mathbf{x}_j, \mathbf{z})\rangle_{L^2(\Gamma)}\right|\left(\max\left|\sum_{n=1}^{N} \langle u^s(\mathbf{x}_j; k), \Phi(\mathbf{x}_j, \mathbf{z})\rangle_{L^2(\Gamma)}\right|\right)^{-1} \tag{8}$$

This approach improves the imaging by DSM. A careful analysis of $\mathcal{I}_{\mathrm{MF}}(\mathbf{z})$ will appear in the extended study.

4. Numerical experiments
To test the proposed approach, we performed diverse numerical experiments on synthetic and experimental single- and multi-frequency data.

4.1. Synthetic data

In the numerical experiments on synthetic data, we consider the imaging of small dielectric inclusions in a homogeneous space by DSM. We explored two cases; varying the properties (size and permittivity) of the inclusions and maintaining the same properties (size and permittivity) of the inclusions.

We assumed that there exist three small dielectric inclusions $\tau = \bigcup_m \tau_m \subset \mathbb{R}^2$, $m = 1, 2, 3$ located at $\mathbf{y}_1 = (0.3, -0.3)$, $\mathbf{y}_2 = (-0.4, -0.2)$, and $\mathbf{y}_3 = (-0.3, 0.5)$. $J = 30$ receivers are placed at $\mathbf{x}_j \in \Gamma$, where Γ is a circle with radius 5 centered at the origin. We assume a single propagation direction, $\mathbf{d} = (1, 1)/\sqrt{2}$. In the single-frequency application, we set $k = 2\pi/\lambda$ with $\lambda = 0.4$; in the multiple-frequency application, we set $k_n = 2\pi/\lambda_n$, where $\lambda_1 = 0.7$ and $\lambda_N = 0.4$ with $N = 10$. Here, λ_n are uniformly distributed in the interval $[0.4, 0.7]$.

(a) Example 4.1   (b) Example 4.2   (c) Example 4.3
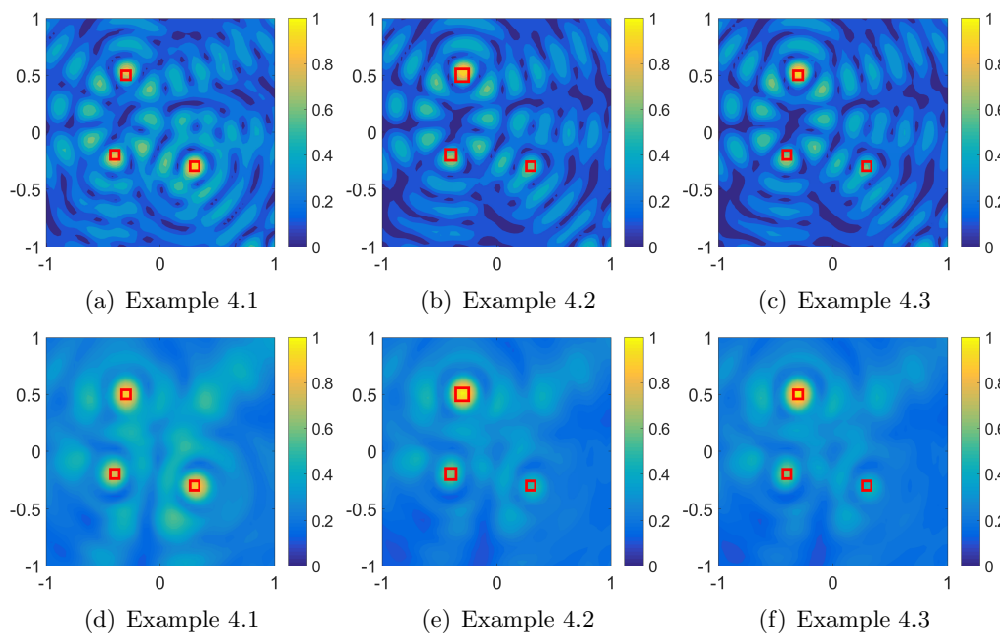
(d) Example 4.1   (e) Example 4.2   (f) Example 4.3

Figure 1. Imaging results of synthetic data: Single-frequency DSM (Top line) and multi-frequency DSM (Bottom line)

Example 4.1 (Case of $\boldsymbol{\alpha_m = \alpha_{m'}}$ and $\boldsymbol{\varepsilon_m = \varepsilon_{m'}}$) *We first set $\alpha_m = 0.1\lambda$ and $\varepsilon_m = 3$ for all $m = 1, 2, 3$. As shown in Figure 1(a), the locations of all inclusions are certificated with high accuracy. In (7), we confirmed that the value of $\mathcal{I}_{\mathrm{SF}}(\mathbf{z}; k)$ depends on the permittivities and sizes of the inclusions. As the permittivities and radii of all inclusions are identical in this case, $\mathcal{I}_{\mathrm{SF}}(\mathbf{z}; k)$ is maximized at $\mathbf{y}_m$, $m = 1, 2, 3$. As expected, the application of multiple frequencies reduces the artifacts; therefore, all inclusions are easily identified (see Figure 1(d)).*

Example 4.2 (Case of $\boldsymbol{\alpha_m \neq \alpha_{m'}}$ and $\boldsymbol{\varepsilon_m = \varepsilon_{m'}}$) *We then set $\alpha_1 = 0.1\lambda$, $\alpha_2 = 0.12\lambda$, and $\alpha_3 = 0.14\lambda$ and maintained the permittivity as $\varepsilon_m = 3$ for $m = 1, 2, 3$. In this case, the value of $\mathcal{I}_{\mathrm{SF}}(\mathbf{z}; k)$ depends only on the sizes of the inclusions. Because τ_3 is larger than the other inclusions, $\mathcal{I}_{\mathrm{SF}}(\mathbf{z}; k)$ is maximized at $\mathbf{y}_3 \in \tau_3$. Meanwhile, the values of $\mathcal{I}_{\mathrm{SF}}(\mathbf{z}; k)$ at $\mathbf{y}_1 \in \tau_1$ and $\mathbf{y}_2 \in \tau_2$ are smaller than that at $\mathbf{y}_3 \in \tau_3$. Therefore, the locations of τ_1 and τ_2 are not easily clarified (see Figure 1(b)). Fortunately, the locations of all inclusions are identifiable in the map of $\mathcal{I}_{\mathrm{MF}}(\mathbf{z})$ (Figure 1(e)).*

Example 4.3 (Case of $\alpha_m = \alpha_{m'}$ and $\varepsilon_m \neq \varepsilon_{m'}$) *In this case, we set $\varepsilon_1 = 3$, $\varepsilon_2 = 4$, and $\varepsilon_3 = 5$, maintaining the radius at $\alpha_m = 0.1\lambda$ for $m = 1, 2, 3$. The imaging result is exhibited in Figure 1(c). As all inclusions have the same radius, the value of $\mathcal{I}_{SF}(\mathbf{z}; k)$ depends only on the permittivities of the inclusions. This means that similar to the results in Example 4.2, the locations of τ_1 and τ_2 are not easily certificated. Fortunately, the multiple-frequency applications guarantee a good result in this case (see Figure 1(f)).*

4.2. Experimental data

Next, we applied DSM to a small U-shaped structure constructed from a metallic material. The experimental data of this structure were borrowed from [11]. We considered the cases of one transmitter ($50°$, $140°$, $230°$, and $320°$), four transmitters, and a full set of transmitters (36 transmitters, $0° \sim 360°$ with step size $10°$). The single-frequency DSM was applied at 8 GHz and the multi-frequency DSM used seven frequencies ranging from 4 to 16 GHz with a step size of 2 GHz. The imaging results of the single- and multi-frequency applications are exhibited in Figures 2 and 3, respectively.
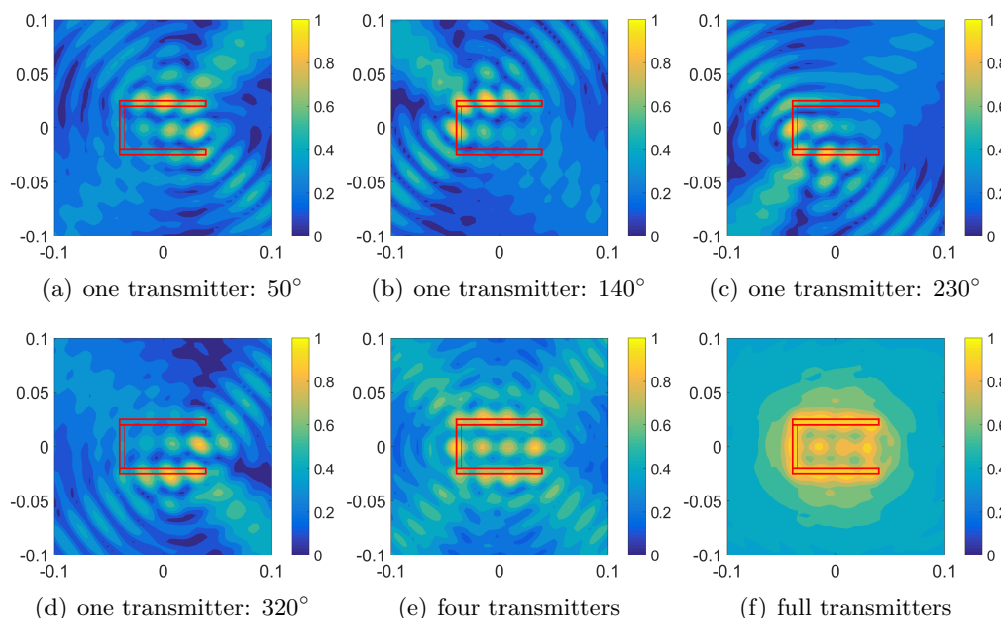

(a) one transmitter: $50°$ (b) one transmitter: $140°$ (c) one transmitter: $230°$

(d) one transmitter: $320°$ (e) four transmitters   (f) full transmitters

Figure 2. Imaging results of experimental data: Single-frequency DSM at 8 GHz

The location and shape of the inclusion are difficult to identify in the single transmitter case (see panels (a), (b), (c), and (d) of Figure 2). In the case of four transmitters, the shape is outlined but remains unclear (Figure 2(e)). In the full-transmitters case, the shape of the material is well clarified (Figure 2(f)). Unlike the results of the synthetic experiment, although our method reduces the artifacts, it does not fully recognize the shape of the material, as shown in Figure 3(a)–(e). Now, we compare the imaging from DSM with full transmitters and one from level set method with single-frequency(see (a) and (b) of Figure 4). Even though level set method is accurate, and efficient techniques, it requires more steps to construct shape like appropriate velocities for advancing the level set function.

5. Conclusion

In this study, we applied single- and multi-frequency DSMs to synthetic and experimental data. From the representative formula of the DSM imaging function and the results of
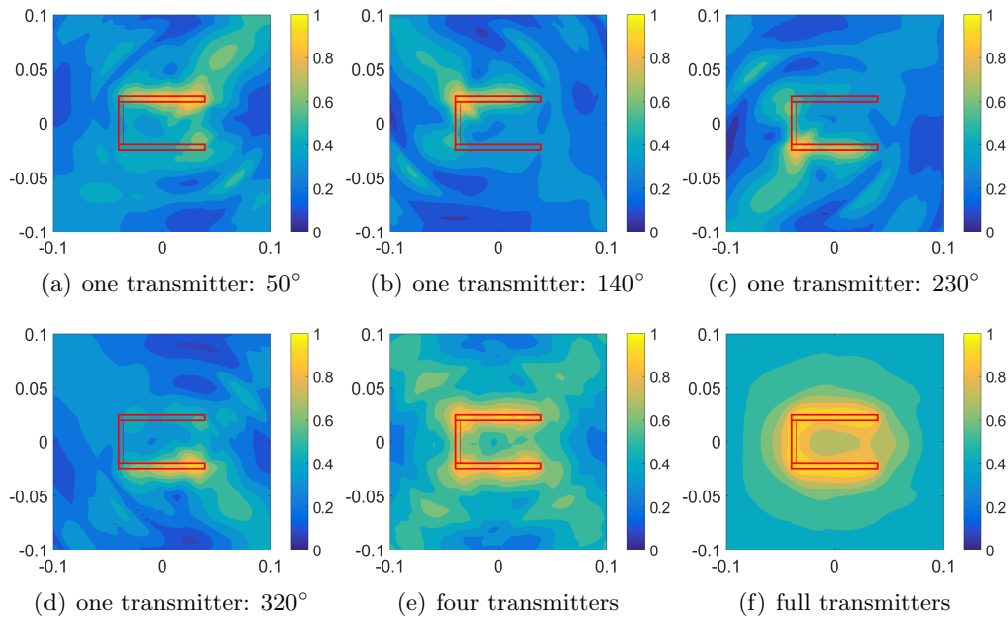
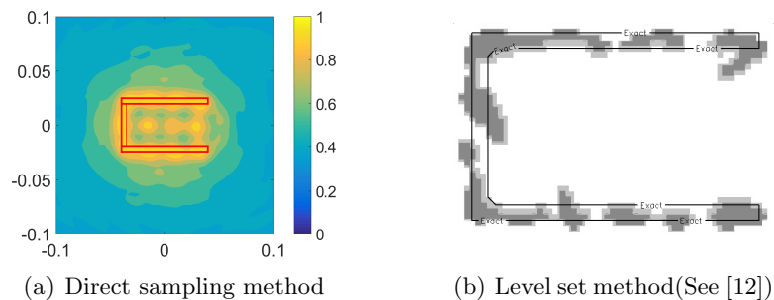**Figure 3.** Imaging results of experimental data: Multi-frequency DSM

Figure 4. Comparison between DSM and Level set method with experimental data at 8 GHz

numerical experiments, we confirmed that our DSM reasonably images synthetic data but requires improvement on experimental data. Identifying the cause of this non-ideal performance and improving our technique will be a forthcoming work. Recently, we found that the DSM is highly related to Kirchhoff migration. Establishing this relation would be an interesting project.

References

[1] Ammari H, Iakovleva E and Lesselier D 2006 *Multiscale Model. Sim.* **3** 597–628
[2] Ammari H, Iakovleva E, Lesselier D and Perrusson G 2007 *SIAM J. Sci. Comput.* **29** 674–709
[3] Cakoni F and Colton D 2003 *Inverse Prob.* **19** 279–295
[4] Colton D, Haddar H and Monk P 2002 *SIAM J. Sci. Comput.* **24** 719–731
[5] Ammari H, Garnier J, Kang H, Park W K and Sølna K 2011 *SIAM J. Appl. Math.* **71** 68–91
[6] Park W K 2015 *J. Comput. Phys.* **283** 52–80
[7] Ito K, Jin B and Zou J 2012 *Inverse Prob.* **28** 025003
[8] Ito K, Jin B and Zou J 2013 *Inverse Prob.* **29** 095018
[9] Li J and Zou Z 2013 *Inverse Probl. Imag.* **7** 757–775
[10] Ammari H and Kang H 2004 *Reconstruction of Small Inhomogeneities from Boundary Measurements* (*Lecture Notes in Mathematics* vol 1846) (Berlin: Springer-Verlag)
[11] Belkebir K and Saillard M 2001 *Inverse Prob.* **17** 1565–1571
[12] Ramananjaona C, Lambert M and Lesselier D 2001 *Inverse Problems* **17** 1585–1595